International Journal of Heat and Technology
Vol. 40, No. 2, April, 2022, pp. 549-560
Journal homepage: http://iieta.org/journals/ijht

Soret-Driven Convection of Non-Newtonian Binary Fluids in a Shallow Cavity Uniformly Heated from Below: Case of Opposing Flows

Khadija Bihiche*, Mohamed Lamsaadi

Research Laboratory in Physics and Sciences for Engineers, Sultan Moulay Slimane University, B.P. 592, Beni-Mellal, Morocco

Corresponding Author Email: khadija.bihiche@gmail.com

https://doi.org/10.18280/ijht.400223

Received: 1 February 2022
Accepted: 20 April 2022

Keywords:
Soret-driven convection, buoyancy ratio, finite volume method, heat and mass transfers, non-Newtonian fluids

ABSTRACT

The project under study investigates Soret-generated convection in a horizontal rectangular cavity filled with a non-Newtonian binary fluid. The cavity's two horizontal walls are exposed to uniform fluxes of heat, whereas the two vertical walls are adiabatic and impermeable. The study focuses on the effects of different key parameters, including the cavity aspect ratio (A), the Lewis number (Le), the buoyancy ratio (N), the power-law behavior index (n), the generalized Prandtl (Pr) and thermal Rayleigh (Ra_T) numbers. The mathematical model, describing the Soret-generated convection phenomenon, is presented by non-linear differential equations, which are solved numerically on the basis of finite volume method. An analytical solution of the problem is proposed derived from the parallel flow approximation in the core of the cavity. The degree of agreement of the numerical finding and analytical predictions is seen to be good. Representative results for the central stream function, Nusselt and Sherwood numbers as well as streamlines, isotherms and iso-concentrations are depicted as functions of the main parameters mentioned above. For opposing flows, the initiation and development of convective motion are explored. The fluid flow's behavior was discovered to be highly influenced by the values of n and N. The beginning of motion is predicted to be governed by supercritical and subcritical Rayleigh numbers.

1. INTRODUCTION

Thermal diffusion or the Soret effect appears when a mixture is exposed to a temperature gradient. A mass flow is a result of a thermal gradient as a response of the system. Analytical and numerical investigations of the Soret effect have revealed that this phenomenon exhibits much more varied behavior in convective motions. This type of convective transport has attracted the interest of researchers for several decades because of its significance in a variety of natural and engineering processes. In nature, we can mention, on a non-exhaustive basis, the convective movements encountered in the oceans and the operation of solar ponds. The most recurrent applications of this phenomenon in industry include processes for the extraction of fluids in oil and natural gas deposits, separation processes in the chemical industry, the underground diffusion of nuclear waste and other contaminants, melting and solidification binary alloys, water desalination operations, crystal growth, etc.

The majority of research on this topic focuses on the Soret-generated convection of a horizontal cavity. Bahloul et al. [1] and Bourich et al. [2] studied analytically and numerically the initiation and development of subcritical and supercritical convection in a horizontal porous layer subjected to uniform densities of heat and mass fluxes at its horizontal walls. For the same configuration, Bourich et al. [3] applied a magnetic field on the Soret convection. They used linear stability to determine the limits of subcritical, Hopf and stationary convection, where various flow patterns may arise. It was found that the magnetic buoyancy forces limit heat transfer rate. However, it can enhance or reduce mass transfer depending on the values of the Hartmann number. Rebhi et al. [4] investigated the same problem taking into account the Dufour effect. Their results show that the Soret and Dufour parameters affect greatly the heat and mass transfer rates. The magnetic flux delays the onset of motion. Alloui et al. [5] have taken up the same problem in pure fluid media. They predicted numerically the critical Rayleigh number for the start of Hopf's bifurcation using stability analysis and the critical Rayleigh number for the start of convection were anticipated by the asymptotic model. In the same spirit, Lagra et al. [6] analyzed Soret-Dufour effects on thermosolutal convection. Recently, Filahi et al. [7] also studied the effect of Soret and Dufour parameters on double diffusive convection in rectangular horizontal Brinkman porous cavity with an undeformable free top surface, whereas the other walls are rigid. They declared that the Soret and Dufour parameters affect strongly the strength of convection and the corresponding heat and solute transfer rates. Mansour et al. [8] investigated the problem of double diffusive instability in the same geometry subjected to vertical fluxes of heat and solute. They investigated the particular case where the imposed heat flux on the sides of the cavity is equilibrated by the thermal-diffusion effects. It was found that the lateral heating has a significant impact on flow and heat transmissions, but it has no influence on mass transfer. Wang et al. [9] analyzed numerically the impact of Dufour and Soret parameters in the same geometry submitted to the high temperature and

concentration on its bottom wall. They demonstrated that the average Nusselt and Sherwood numbers increase with increase of Soret and Dufour coefficients. Wang et al. [10] studied the flow structure and the heat and mass transfers of thermosolutal convection in the same cavity with coupling-diffusion interaction under varying Rayleigh number and buoyancy ratio. They showed that the Nusselt and Sherwood numbers increased linearly with Soret and Dufour coefficients, particularly for high Rayleigh numbers. Another study of the Soret-driven convection was investigated by Charrier-Mojtabi et al. [11] in a porous cavity submitted to uniform but various temperatures on its long surfaces using stability analysis. They concluded that the stability of mechanical equilibrium solution depends on the normalized porosity and the separation ratio. As a result, the equilibrium solution was strongly affected by the normalized porosity and the separation ratio. Recently Mojtabi [12] developed a new process developing the species separation of a binary medium under microgravity by using a rectangular layer. The resulting convection of a binary fluid was engendered by regular velocities applied on the two horizontal walls of the layer that are subjected to constant but different temperatures. As a result, the species separation is is much enhanced compared to that of thermo-gravitational vertical columns (TGC). Mutschler and Mojtabi [13] extended the problem of Soret-generated convection in a horizontal porous layer filled with a binary fluid to an n-component mixture. The first part of the paper included an analytical and numerical investigation of the onset of Soret-generated convection. The research was based on the Darcy-Boussinesq equations, which allowed for a mechanical solution in the pure double-diffusive regime. The separation was expressed in terms of the governing parameters of the problem in the second portion, which included the asymptotic solution for the unicellular flow.

Indeed, in the most of the chemical and allied processing industries, the fluid flow shows a non-Newtonian behavior. Considerable efforts have been devoted to the analysis of various convection processes in non-Newtonian fluids, although the results obtained are still few compared to that of the Newtonian case. Benhadji and Vasseur [14] used the Darcy model to investigate the double-diffusive convection flows in rectangular layer saturated with a power-law fluid saturated porous medium. The cavity is supposed heated and salted from all boundaries. They examined the effect of the main governing parameters including thermal Rayleigh number, Lewis number and buoyancy ratio on the strength of convection and heat and mass transfer characteristics. The onset of double-diffusive and Soret-generated convection in the same geometry heated and salted from below was investigated by Khelifa et al. [15]. The reported results show that the flow behavior is highly influenced by the value of power-law index and buoyancy ratio. The onset of convection is supercritical for a dilatant fluid for aiding buoyancy forces while it is subcritical for opposing buoyancy ratio. Convection occurs via subcritical bifurcation for a pseudo-plastic one independently of the value of buoyancy ratio. In pure fluid media, Rebhi et al. [16] focused on the study of bistability of bifurcation in the same geometry filled with a non-Newtonian fluid obeying Carreau-Yassuda model. They showed that the bistability convection is influenced by the buoyancy ratio. Saeed et al. [17] investigated double-diffusive transport in Casson fluid flows under magnetic field. It has been demonstrated that changing the fluid properties, the magnetic field, and its angle of incidence greatly increases the Nusselt number in the thin-wall limit. In this sense, Amari et al. [18] published an analytical and numerical study of non-Newtonian fluid natural convection in a horizontal porous layer heated from the side-walls, or from the horizontal ones. The flow and temperature fields, as well as the Nusselt numbers, are clearly expressed in terms of the modified Rayleigh number and the power-law index. It was found that the velocity fields and the temperature distribution, as well as the Nusselt numbers, are affected by the power-law index. Recently, Bihiche et al. [19] studied the effects of double-diffusive convection in rectangular enclosure of power-law fluids with lateral heat and mass fluxes. As a result, the existence of a multiple steady states is proved in the case of opposing flows. Recently, Li et al. [20] investigated the bifurcation phenomenon of thermosolutal convection arising when the flow loses its symmetry with an internal thermal and solutal source in a horizontal layer. The results presented show that the symmetry of the system can be destabilized by increasing buoyancy ratio also the strong couple diffusion effect delays the onset of motion. In the case of a square cavity, a numerical study was performed by Makayssi et al. [21] to examine the influence of a magnetic field on natural double-diffusive convection of an electroconductor non-Newtonian binary fluid. Consequently, the magnetic field only appears to have a significant impact on the Nusselt and Sherwood numbers only at moderate thermal Rayleigh numbers.

Kefayati and Tang [22] simulated heat and mass transfer of three dimensional double diffusive natural convection and entropy generation of a non-Newtonian Carreau-Yasuda fluid in a cubic layer. They examined the effect of the main controlling parameters including Carreau number, Carreau-Yasuda parameter, power-law indexes, Lewis number, thermal Rayleigh number and buoyancy ratio on the entropy generations and heat and mass transfers.

It is clear that so far, the resulting natural convection of non-Newtonian fluid confined in rectangular cavity, except for the study carried out by Khelifa et al. [15] in the case of a porous media, the Soret effect have been neglected while it has demonstrated that they have a significant impact on heat and mass transports. Thus, the present study focuses on the problem of the onset of convection and the resulting Soret-generated convection of a non-Newtonian binary fluid in pure fluid rectangular cavity subject to vertical fluxes of heat.

2. MATHEMATICAL FORMULATION OF THE PROBLEM

Figure 1 depicts the flow configuration under study. It consists of a horizontal rectangular layer of height H′ and length L′ saturated with a power-law non-Newtonian binary fluid. The horizontal walls of the cavity are subject to constant fluxes of heat while the short vertical ones are impermeable and adiabatic. The Prandtl number is fixed at Pr = 100.

For a simple formulation of the mathematical model, we will consider some approximations which are often used in the study of natural convection. We then assume that:

- The fluid velocities are low enough that the flow can be classified as laminar. Due to modest temperature gradients, fluid circulation is slow in most buoyancy-driven motions [23].
- The fluid is incompressible. With a good approximation for pressures approaching atmospheric, liquids can be termed incompressible

fluids.

- The work of the viscous forces is negligible. This approach, according to Turki [24], is valid for polymer solutions that are faintly concentrated.
- The cavity's third dimension is large enough to make the problem two-dimensional.
- The thermophysical properties of the considered fluid are constant except for the density for which the Boussinesq approximation remains valid. It depends on both the local temperature and concentration by the state equation:

$$\rho = \rho_0\left[1 - \beta_T(T' - T_c') - \beta_S(S' - S_c')\right]$$

where, ρ_0 is the fluid mixture density at $T' = T_c'$ and $S' = S_c'$ and β_T and β_S are the thermal and concentration expansion coefficients, respectively.

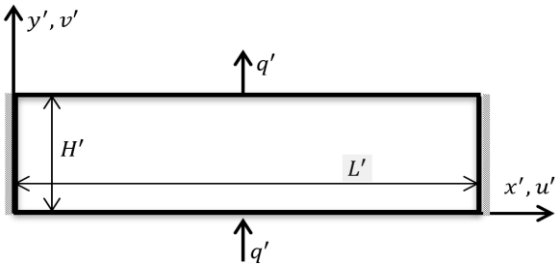

Figure 1. Geometry of the present study

Several mathematical models have been presented in the literature to model the behavior of non-Newtonian fluids. In this work, we are particularly interested in fluids with time-independent behavior and more particularly in dilatant and pseudoplastic fluids. For these types of fluids, the empirical power law model proposed by Ostwald-de Waele (1925) is the most widely adopted in the literature. The following statement expresses this law in the Cartesian coordinates system, in term of laminar apparent viscosity, is,

$$\mu_a' = k\left[2\left[\left(\frac{\partial u'}{\partial x'}\right)^2 + \left(\frac{\partial v'}{\partial y'}\right)^2\right] + \left[\frac{\partial u'}{\partial y'} + \frac{\partial v'}{\partial x'}\right]^2\right]^{\frac{n-1}{2}} \quad (1)$$

where, k and n are two empirical parameters known as the consistency factor and power-law index of the fluid, respectively. It's worth noting that these values have no physical significance. For $0 < n < 1$, the fluid is considered to be pseudo-plastic (or shear-thinning). However, the fluid is referred to be dilatant (or shear-thickening) for $n > 1$. The case n = 1 corresponds to the Classical Newtonian behavior.

Considering the simplifying assumptions stated above, the basic equations governing the flow and the heat and mass transfers within the cavity considered are given by:

$$\frac{\partial u}{\partial x} + \frac{\partial v}{\partial y} = 0 \quad (2)$$

$$\frac{\partial u}{\partial t} + u\frac{\partial u}{\partial x} + v\frac{\partial u}{\partial y} = -\frac{\partial p}{\partial x} + Pr\left[\mu_a\left(\frac{\partial^2 u}{\partial x^2} + \frac{\partial^2 u}{\partial y^2}\right) + 2\frac{\partial \mu_a}{\partial x}\frac{\partial u}{\partial x} + \frac{\partial \mu_a}{\partial y}\left(\frac{\partial u}{\partial y} + \frac{\partial v}{\partial x}\right)\right] \quad (3)$$

$$\frac{\partial v}{\partial t} + u\frac{\partial v}{\partial x} + v\frac{\partial v}{\partial y} = -\frac{\partial p}{\partial y} + Pr\left[\mu_a\left(\frac{\partial^2 v}{\partial x^2} + \frac{\partial^2 v}{\partial y^2}\right) + 2\frac{\partial \mu_a}{\partial y}\frac{\partial v}{\partial y} + \frac{\partial \mu_a}{\partial x}\left(\frac{\partial u}{\partial y} + \frac{\partial v}{\partial x}\right)\right] + Ra_T Pr(T + NS) \quad (4)$$

$$\frac{\partial T}{\partial t} + u\frac{\partial T}{\partial x} + v\frac{\partial T}{\partial y} = \frac{\partial^2 T}{\partial x^2} + \frac{\partial^2 T}{\partial y^2} \quad (5)$$

$$\frac{\partial S}{\partial t} + u\frac{\partial S}{\partial x} + v\frac{\partial S}{\partial y} = \frac{1}{Le}\left[\left(\frac{\partial^2 S}{\partial x^2} + \frac{\partial^2 S}{\partial y^2}\right) - \left(\frac{\partial^2 T}{\partial x^2} + \frac{\partial^2 T}{\partial y^2}\right)\right] \quad (6)$$

Solving the system of the Eqns. (2)-(6), requires a certain number of boundary conditions defined as follows:

$$u = v = 0\,, \frac{\partial T}{\partial x} = \frac{\partial S}{\partial x} = 0 \text{ for } x = 0 \text{ and } A \quad (7)$$

$$u = v = 0, \frac{\partial T}{\partial y} = -1, \frac{\partial S}{\partial y} = \frac{\partial T}{\partial y} = -1 \text{ for } y = 0 \text{ and } 1 \quad (8)$$

where, μ_a is the dimensionless apparent viscosity, that is defined for the two-dimensional Cartesian coordinates as:

$$\mu_a = \left[2\left[\left(\frac{\partial u}{\partial x}\right)^2 + \left(\frac{\partial v}{\partial y}\right)^2\right] + \left[\frac{\partial u}{\partial y} + \frac{\partial v}{\partial x}\right]^2\right]^{\frac{n-1}{2}} \quad (9)$$

The flow pattern can be examined by introducing the stream function, ψ, defined as:

$$u = \frac{\partial \psi}{\partial y} \text{ and } v = -\frac{\partial \psi}{\partial y} (\psi = 0 \text{ on all boundaries}) \quad (10)$$

The dimensionless control parameters that appear are:

$$A = \frac{L'}{H'}\,, Le = \frac{\alpha}{D}, N = \frac{\beta_S \Delta S^*}{\beta_T \Delta T^*}, Pr = \frac{\left(\frac{k}{\rho}\right) H'^{2-2n}}{\alpha^{2-n}} \text{ and } Ra_T = \frac{g\beta_T H'^{2n+2} q'}{(k/\rho)\alpha^n \lambda} \quad (11)$$

The group A is the aspect ratio of the enclosure. The Lewis number Le compares the mass diffusivity with the thermal diffusivity. The buoyancy ration N is a measure of the relative contribution of concentration and thermal diffusion to the variation of the density which drives convective flow. The two last dimensionless groups are the Prandtl and thermal Rayleigh numbers, respectively.

The Newtonian expressions for Pr and Ra_T are obtained by setting in the above expressions n = 1 and k = μ.

The local Nusselt and Sherwood numbers are defined to express the heat and mass transports. They are defined as follows:

$$\overline{Nu} = \frac{1}{A}\int_0^1 \frac{1}{\Delta T(x)}\,dy \text{ and } \overline{Sh} = \frac{1}{A}\int_0^1 \frac{1}{\Delta S(x)}\,dy \qquad (12)$$

where, $\Delta T(x) = T(x,0) - T(x,1)$ and $\Delta S(x) = S(x,0) - S(x,1)$ are the dimensionless local temperature and concentration differences.

3. NUMERICAL SOLUTION

The governing equations (2)-(6) related to the boundary conditions (7)-(8), are solved numerically on the basis a finite volume method using SIMPLER algorithm [25]. Thereafter, the discretized equations for each control volume in the flow domain can be solved easily by a generalization of the tridiagonal matrix (TDMA) algorithm with relaxation. The solution procedure is repeated until the convergence criteria is attained when $\sum_{i,j}\left|f_{i,j}^{k+1} - f_{i,j}^{k}\right| < 10^{-5}\sum_{i,j}\left|f_{i,j}^{k+1}\right|$, where $f_{i,j}^{k}$ represents the value of u, v, p, T or S at the node (i, j) for the k^{th} iteration level in the plane (x, y).

The effects of the flow behavior index, n, on the flow structure, temperature and concentration distributions, are illustrated in Figure 2 for A = 24, Pr = 100, Le = 2, N = -0.02, $Ra_T = 10^3$. It should be noted that the resulting flow pattern can be either clockwise or counterclockwise. The numerical results presented here were obtained for the positive value of ψ_C. As can be seen from this figure, it is clear that isotherms and iso-concentrations become less inclined, while decreasing n, which proves, thus, that the flow intensity is a decreasing function of power-law index, n.

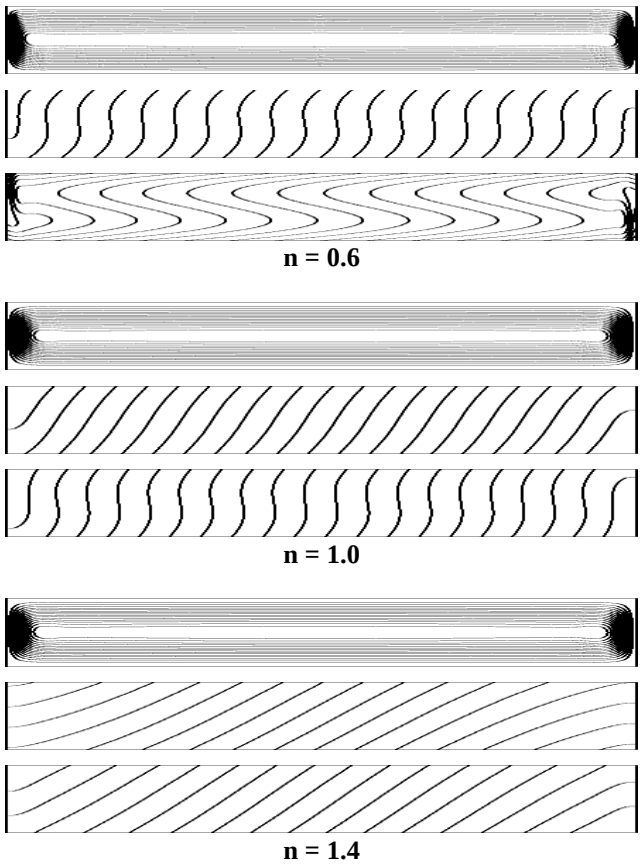

Figure 2. Streamlines (top), isotherms (middle) and iso-concentrations (bottom) for A = 24, Pr = 100, Le = 2, N = -0.02, $Ra_T = 10^3$ and different power-law indexes values of n

Several tests, for different mesh sizes, are carried out in similar conditions for the purpose of determining the suitable grid field to conduct accurately the present study in terms of running time and precision of the computations.

Hence, the grid size of 381x121 is jugged sufficient to model accurately the present study with an aspect ratio A = 24. The values of time-step are varied from 10^{-5} to 10^{-3}, depending on the controlling parameters of the study. The present numerical code can be validated for the case studied by Alloui et al. [5] for the particular case of Newtonian fluid (the convection induced purely by Soret effect can be found by replacing j = 0 in the reference of Alloui et al. [5]. In this case, the results obtained by our code are brought to the same conditions held by the reference). The numerical results obtained by these authors as well as our results are grouped in Table 1. The comparison between these results shows that the maximum error is around 4%. In addition, the analytical solution which will be discussed in the next section also made it possible to validate the numerical code.

Table 1. Validation of the numerical code, for n = 1, in terms of ψ_{max}, $\overline{Nu}$ and $\overline{Sh}$

Alloui et al. (2010)			Present study		
ψ_{max}	$\overline{Nu}$	$\overline{Sh}$	ψ_{max}	$\overline{Nu}$	$\overline{Sh}$
1.29	1.29	3.20	1.24	1.284	3.197

4. PARALLEL FLOW ANALYSIS

The numerical results illustrated in Figure 2 show that the flow is parallel in the central part of the enclosure, i.e. v = 0, thus we have:

$$\begin{aligned}\psi(x,y) = \psi(y), u(x,y) = u(y)\ T(x,y) &= C_T(x - A/2) \\ &+ \theta_T(y) \text{ and } S(x,y) \\ &= C_S(x - A/2) + \theta_S(y)\end{aligned} \qquad (13)$$

where, C_T and C_S are unknown constant temperature and concentration gradients respectively, in the *x*-direction (see for instance Refs. [21, 26, 27]). On the basis of these simplifications, Eqns. (2)-(6) reduce to the following systems of equations:

$$\frac{d^2}{dy^2}\left[\left|\frac{du(y)}{dy}\right|^{n-1}\frac{du(y)}{dy}\right] = (C_T + NC_S)Ra_T \qquad (14)$$

$$\begin{aligned}\frac{d^2\theta_T(y)}{dy^2} = C_T u(y) \text{ and } \frac{d^2\theta_S(y)}{dy^2} \\ = (LeC_S + C_T)u(y)\end{aligned} \qquad (15)$$

$$u = 0, \frac{d\theta_T}{dy} = -1, \frac{d\theta_S}{dy} = \frac{d\theta_T}{dy} = -1 \text{ for } y = 0 \text{ and } 1 \qquad (16)$$

with

$$\int_0^1 u(y)dy = 0, \int_0^1 \theta_T(y)dy = 0 \text{ and } \int_0^1 \theta_S(y)dy = 0 \qquad (17)$$

as return flow and mean temperature and concentration conditions, respectively (see for instance Refs [21, 26]).

Because of the high coupling and nonlinear character of the governing equations, integrating Eqns. (14) and (15) with conditions (16) and (17) is difficult and necessitates a particular numerical approach. In reality, due to the non-linear rheological effect of the fluid behavior and the change in the velocity gradient sign, the velocity expressions alter depending on whether $0 \le y \le y_0$, $y_0 \le y \le y_1$ or $y_1 \le y \le 1$ where y_0 and y_1 are the y-coordinates for which $du/dy = 0$. They are obtained from Eq. (17), which is numerically resolved by combining Gauss-Legendre integration and Regula-Falsi iteration methods [28, 29]. The function $f(y) = (y^2 - y + y_0 y_1)/2$ is introduced to simplify the velocity, temperature, and concentration expressions. As a result, $u(y)$, $\theta_T(y)$ and $\theta_S(y)$ can be expressed as:

$$u(y) = Ra_T^{1/n}(C_T + NC_S)^{1/n} F(y) \tag{18}$$

$$\theta_T(y) = C_T Ra_T^{1/n}(C_T + NC_S)^{1/n}\left[G(y) - \int_0^1 G(y)dy\right] - \left[y - \frac{1}{2}\right] \tag{19}$$

$$\theta_S(y) = \frac{LeC_S + C_T}{C_T}\theta_T(y) + \left[\frac{(LeC_S + C_T)}{C_T}\right]\left[y - \frac{1}{2}\right] \tag{20}$$

where, the functions $F(y)$ and $G(y)$ are defined as:

- $0 \le y \le y_0$

$$F(y) = \int_0^y [f(y)]^{1/n} dy \tag{21}$$

$$G(y) = \int_0^y \left[\int_0^y \left[\int_0^y [f(y)]^{\frac{1}{n}} dy\right] dy\right] dy \tag{22}$$

- $y_0 \le y \le y_1$

$$F(y) = \int_0^{y_0} [f(y)]^{1/n} dy + \int_y^{y_0} [-f(y)]^{1/n} dy \tag{23}$$

$$\begin{aligned} G(y) = {} & \frac{(y - y_0)^2}{2}\int_0^{y_0} [f(y)]^{\frac{1}{n}} dy \\ & + \int_{y_0}^{y} \left[\int_{y_0}^{y} \left[\int_{y}^{y_0} [-f(y)]^{\frac{1}{n}} dy\right] dy\right] dy \\ & + (y - y_0)\int_0^{y_0} \left[\int_0^{y} [f(y)]^{\frac{1}{n}} dy\right] dy \\ & + \int_0^{y_0} \left[\int_0^{y} \left[\int_0^{y} [f(y)]^{1/n} dy\right] dy\right] dy \end{aligned} \tag{24}$$

- $y_1 \le y \le 1$

$$\begin{aligned} F(y) = {} & \int_0^{y_0} [f(y)]^{\frac{1}{n}} dy \\ & + \int_{y_1}^{y} [-f(y)]^{\frac{1}{n}} dy \\ & + \int_{y_1}^{y} [f(y)]^{1/n} dy \end{aligned} \tag{25}$$

$$\begin{aligned} G(y) = {} & \frac{1}{2}(y - y_1)(y + y_1 \\ & - 2)\left[\int_0^{y_0} [f(y)]^{\frac{1}{n}} dy \right. \\ & \left. + \int_{y_1}^{y_0} [-f(y)]^{\frac{1}{n}} dy\right] \\ & + \int_{y_1}^{y} \left[\int_1^{y} \left[\int_{y_1}^{y} [f(y)]^{\frac{1}{n}} dy\right] dy\right] dy \\ & + \frac{1}{2}(y_1 - y_0)^2 \int_0^{y_0} [f(y)]^{\frac{1}{n}} dy \\ & + (y_1 - y_0)\int_0^{y_0} \left[\int_0^{y} [f(y)]^{\frac{1}{n}} dy\right] dy \\ & + \int_{y_0}^{y_1} \left[\int_{y_0}^{y} \left[\int_{y}^{y_0} [-f(y)]^{\frac{1}{n}} dy\right] dy\right] dy \\ & + \int_0^{y_0} \left[\int_0^{y} \left[\int_0^{y} [f(y)]^{1/n} dy\right] dy\right] dy \end{aligned} \tag{26}$$

At this stage, it is advisable to introduce the current function at the center of the cavity in order to be able to measure the intensity of the convection. Its expression can be deduced simply by integrating Eq. (10) and considering the associated boundary conditions. We then obtain:

$$\psi_c = \psi\left(y = \frac{1}{2}\right) = \frac{Ra_T^{1/n}(C_T + NC_S)^{1/n}}{D_n} \tag{27}$$

where,

$$\begin{aligned} D_n = {} & \left[\left(\frac{1}{2} - y_0\right)\int_0^{y_0} [f(y)]^{1/n} dy \right. \\ & + \int_0^{y_0} \left(\int_0^{y} [f(y)]^{1/n} dy\right) dy \\ & \left. + \int_{y_0}^{1/2} \left(\int_y^{y_0} [-f(y)]^{1/n} dy\right) dy\right]^{-1} \end{aligned} \tag{28}$$

Therefore, taking into consideration the Eq. (27), $u(y)$, $\theta_T(y)$ and $\theta_S(y)$ can be expressed as:

$$u(y) = D_n \psi_c F(y) \tag{29}$$

$$\theta_T(y) = C_T D_n \psi_c \left[G(y) - \int_0^1 G(y)dy \right] - \left[y - \frac{1}{2} \right] \tag{30}$$

$$\theta_S(y) = Le C_S \theta_T(y) + \left[\frac{Le C_S}{C_T} - 1 \right] \left[y - \frac{1}{2} \right] \tag{31}$$

Obviously, the boundary conditions in the x-direction, given by Eqns. (7) and (8), cannot be fulfilled with the parallel flow solution. It is then necessary, for calculating the gradients C_T and C_S, to make energy and mass balances on a control volume connecting the region of the parallel flow to an edge of the cavity [30]. We then have:

$$\int_0^1 uTdy = \int_0^1 \frac{\partial T}{\partial x} dy \text{ and } Le \int_0^1 uSdy = \int_0^1 \frac{\partial S}{\partial x} dy \tag{32}$$

Using the approximations, Eq. (13), together with the conditions (7) and (8), Eq. (32) becomes:

$$\int_0^1 u\theta_T dy = C_T \text{ and } Le \int_0^1 u\theta_S dy = C_S \tag{33}$$

Substituting Eqns. (29), (30) and (31) into Eq. (33) and integrating, considering the conditions (17), C_T and C_S can be obtained as:

$$C_T = \frac{B_n D_n \psi_c}{1 - A_n (D_n \psi_c)^2} \text{ and } C_S = \frac{Le B_n D_n \psi_c}{(1 - Le^2 A_n (D_n \psi_c)^2)} \tag{34}$$

where,

$$A_n = \int_0^1 F(y)G(y)dy \text{ and } B_n = -\int_0^1 yF(y)dy \tag{35}$$

Thus, when C_T and C_S are replaced with their respective expressions into Eq. (27), we end up with the following transcendental equation:

$$\begin{aligned} &[A_n^2 Le^2 D_n^4 \psi_c^4 - A_n (Le^2 + 1) D_n^2 \psi_c^2 + 1] D_n^n \psi_c^n \\ &\quad + Ra_T [A_n B_n Le^2 D_n^3 \psi_c^3 \\ &\quad - B_n (1 + N + NLe) D_n \psi_c] = 0 \end{aligned} \tag{36}$$

The values of the coefficient An, B_n and D_n are given with those of y_0 in Table 2.

Table 2. Coefficients y_0, A_n, B_n and D_n for different values of n

n	y_0	D_n	A_n	B_n
0.6	0.19915	2904.6982	-0.4849×10^{-7}	0.1860×10^{-3}
0.8	0.20608	824.6777	-0.5998×10^{-6}	0.6507×10^{-3}
1.0	0.21132	383.9999	-0.2756×10^{-5}	0.1389×10^{-2}
1.2	0.21544	229.6020	-0.7679×10^{-5}	0.2310×10^{-2}
1.4	0.21877	158.5755	-0.1604×10^{-4}	0.3330×10^{-2}

The value of ψ_c can be evaluated by solving Eq. (36) with the Newton-Raphson method, and the values of C_T and C_S are determined from Eq. (34), for any combination of the governing parameters Le, N, n and Ra_T.

Finally, considering Eq. (12), the final form of the average Nusselt and Sherwood numbers are as follows:

$$\overline{Nu} = \frac{1}{2\theta_T(0)} \text{ and } \overline{Sh} = \frac{1}{2\theta_S(0)} \tag{37}$$

5. RESULTS AND DISCUSSION

The main purpose of this research is to illustrate the effect of the control parameters on the Nusselt and Sherwood numbers as well as on the flow structure. Several researchers (see for instance Refs. [26, 31, 32]) have demonstrated that the convection is largely immune to Pr variations if this number is large enough. Therefore, Pr is kept at a constant value Pr = 100. The thermal Rayleigh number Ra_T, the power-law index n, the Lewis number Le and the buoyancy ratio N are therefore the parameters regulating the problem.

5.1 Effect of Ra_T and n

The effect of the power law index and thermal Rayleigh number on the onset of motion and heat and mass transfer rates are examined in this section for the case of opposing flows. Figure 3 shows the values of ψ_c versus Ra_T for $-0.5 \le N < 0$ for which the destabilizing thermal influence competes with a stabilizing solutal influence. The behavior of ψ_c depend strongly on the values of N and n and present significant changes as displayed in Figure 3. The case of Newtonian fluid will be discussed first. As observed from Figure 3, for $N \ge N^*$, where $N^* = -0.067$, the pitchfork bifurcation curve is obtained at a supercritical Rayleigh number $Ra_{TC}^{Sup} = 901.1251$ and 742.2693 for $N = -0.067$ and $N = -0.01$, respectively. For $N < N^*$, convection becomes subcritical and occurs with a finite amplitude convection. Thus, the problem presents a multiplicity of solutions for the same value of the governing parameters in comparison with that of $N \ge N^*$. Therefore, the corresponding critical Rayleigh number is now $Ra_{TC}^{Sub} = 1464.028$ and 2015.309 for $N = -0.27$ and $N = -0.5$, respectively. For this particular case, i.e. for n = 1, it can be easily proved that the subcritical Rayleigh number for the start of motion is given by:

$$Ra_{TC}^{Sub} = \frac{A_n^2 Le^2 D_n^4 \psi_{cc}^4 - A_n (Le^2 + 1) D_n^2 \psi_{cc}^2 + 1}{B_n (1 + N + NLe) - A_n B_n (Le^2) D_n^2 \psi_{cc}^2} \tag{38}$$

where,

$$\psi_{cc} = \left[\frac{Le(1 + N + NLe) - [C_1]^{\frac{1}{2}}}{A_n Le^4 D_n^2} \right]^{\frac{1}{2}} \tag{39}$$

where,

$$\begin{aligned} C_1 = {} & Le^2 (1 + N + NLe)^2 + Le^4 \\ & - (Le^2 + 1) Le^2 (1 + N + NLe) \end{aligned} \tag{40}$$

The condition $N < N^*$ must be fulfilled for the presence of subcritical convection. The corresponding results obtained for the case of a dilatant fluid are reported in Figure 3. Here, when

$N \geq N_1^*$, where $N_1^* = -0.2335$, any Rayleigh number greater than zero can cause convection ($Ra_{TC}^{Sup} = 0$). On the other hand, for $N_2^* < N < N_1^*$, where $N_2^* = -0.34$, Ra_{TC}^{Sup} is always zero but the problem now presents three solutions for a given Ra_T. For $N \leq N_2^*$, the convection becomes subcritical. It is also shown that the number of multiple solutions is reduced to two instead of three for a given Ra_T. However, for a pseudoplastic fluid, contrarily to case of Newtonian and dilatant fluids, ψ_c presents the same behavior whatever the value of N. In fact, as it can be seen from Figure 3, convection occurs as a result of a subcritical bifurcation for all the selected value of N. It should be pointed out that, for all graphs of this study, the analytical solution represented by the solid (stable solution) agree closely with numerical predictions depicted by blackened symbols. Numerical solutions for the unstable branch were not available (dashed line). Figures 4 and 5 illustrate the corresponding Nusselt and Sherwood numbers, $\overline{Nu}$ and $\overline{Sh}$, as a function of Ra_T, for Le = 2, N = -0.5 and different value of n. Here again, the analytical predictions agree well with the numerical simulations. It is observed that convection is only attainable if the Rayleigh number reaches a subcritical value $Ra_{TC}^{Sub} =$ 528.19, 2015.309 and 7061.414 for n = 0.6, 1 and 1.4 respectively. Here again, the analytical predictions agree well with the numerical simulations.

It is observed from this figure that, $\overline{Nu}$ increases by increasing Ra_T while $\overline{Sh}$ increases considerably at the beginning with Ra_T until it reaches a maximum, for a given value of Ra_T, then decreases to reach an asymptotic value.

The profile of horizontal velocity at the mid-length of the layer (x = A/2) is shown in Figure 6. It is noticed that the numerical simulations agree well with their analytical counterparts. It is noted also from Figure 6 that, for the parameters considered here, the rest state is reached only for the case of Newtonian fluid and it is never reached for a dilatant and pseudoplastic fluid, which is in agreement with the results obtained above. In fact, for the parameters considered here, namely Le = 2, Ra_T = 901.125, n = 1 and different values of N such as $0 < N \leq -0.5$. The corresponding buoyancy ratio for the start of motion is given by N = -0.067 as predicted by Eq. (38). Thus, the start of motion is conditioned by N < -0.067.

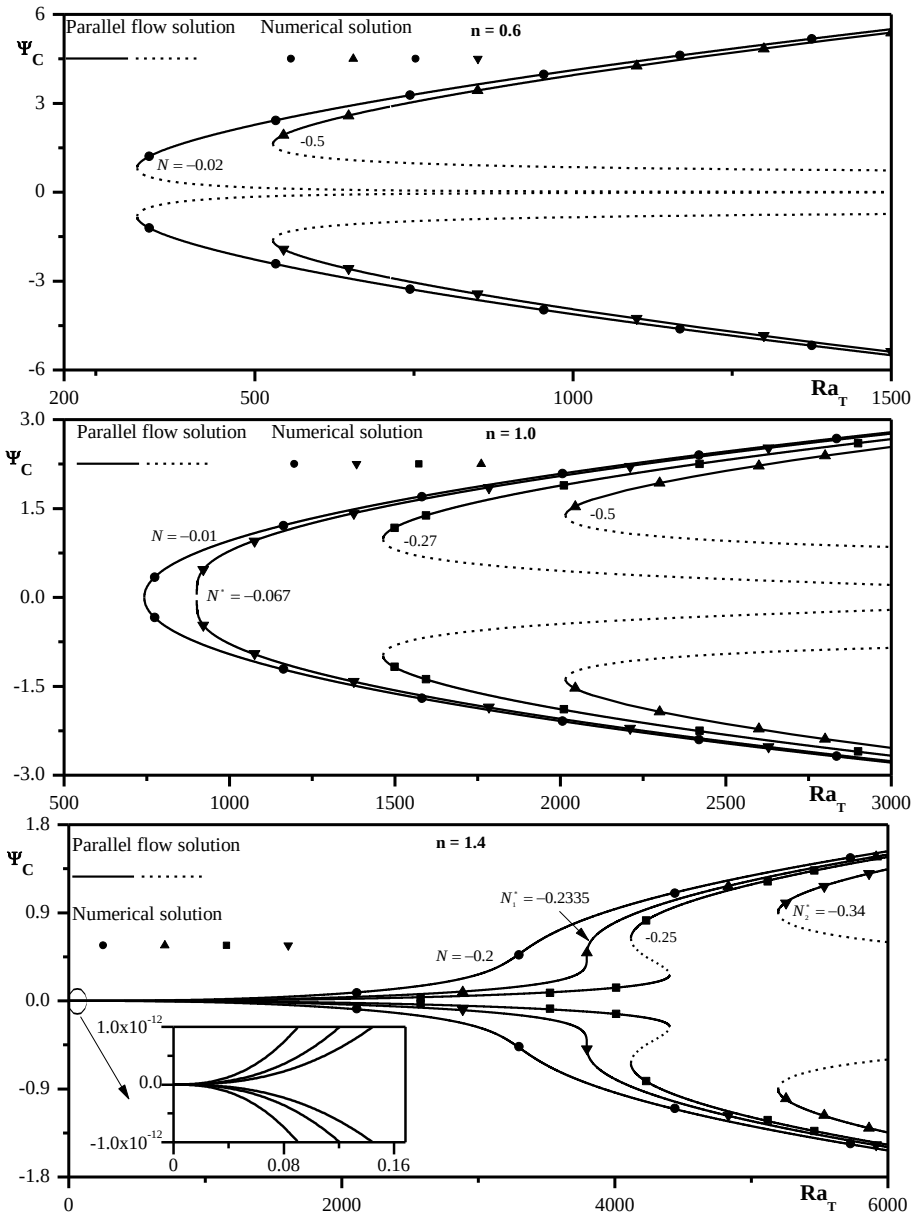

Figure 3. Bifurcation diagram in term of ψ_C versus Ra_T for Le = 2 and different values of n and N

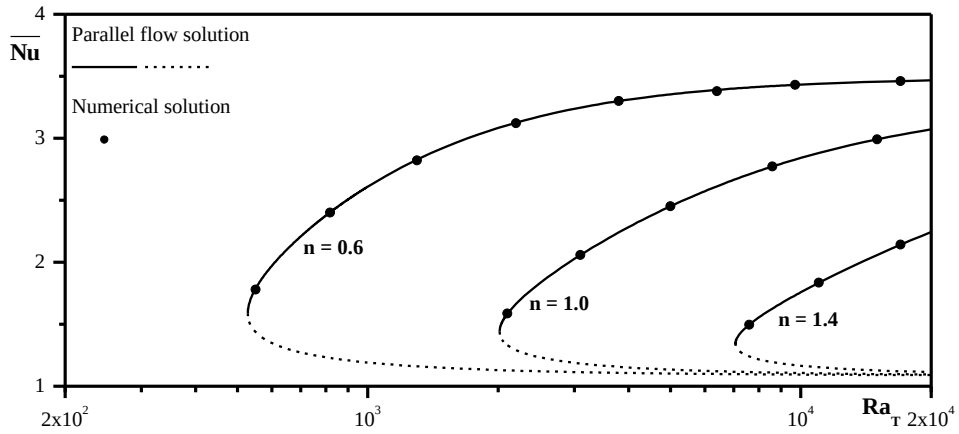

Figure 4. Bifurcation diagram in term of $\overline{Nu}$ versus Ra_T for Le = 2, N = -0.5 and different values of n

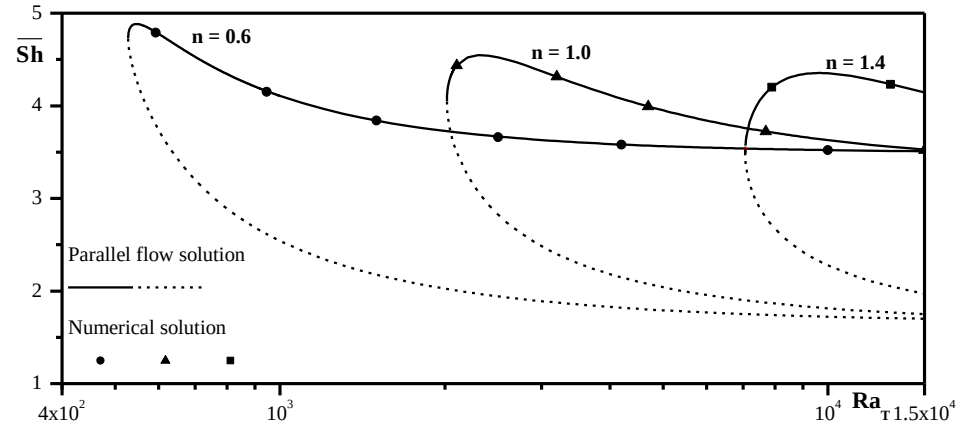

Figure 5. Bifurcation diagram in term of $\overline{Sh}$ versus Ra_T for Le = 2, N = -0.5 and different values of n

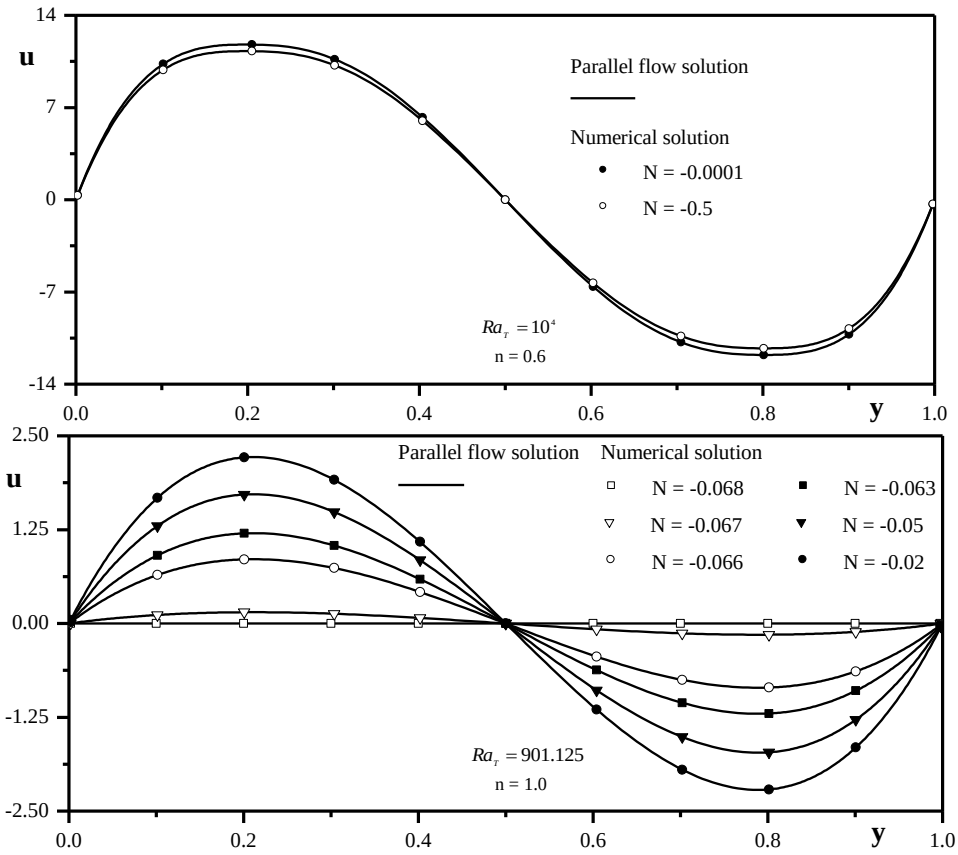

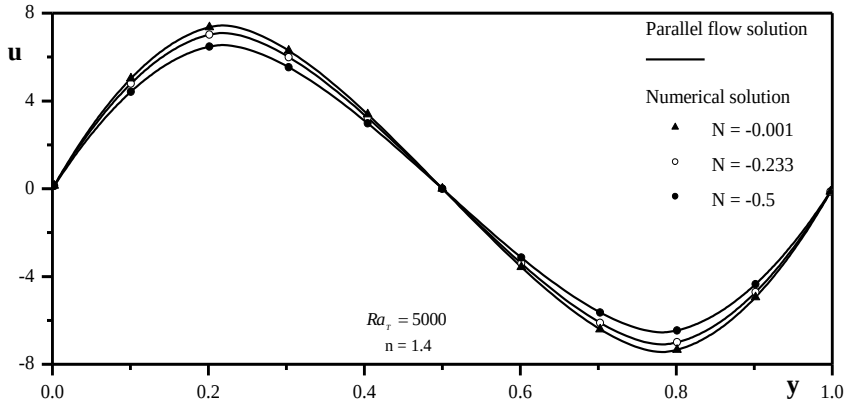

Figure 6. Effect of N on the horizontal velocity profiles for Le = 2 and different values of n and Ra_T

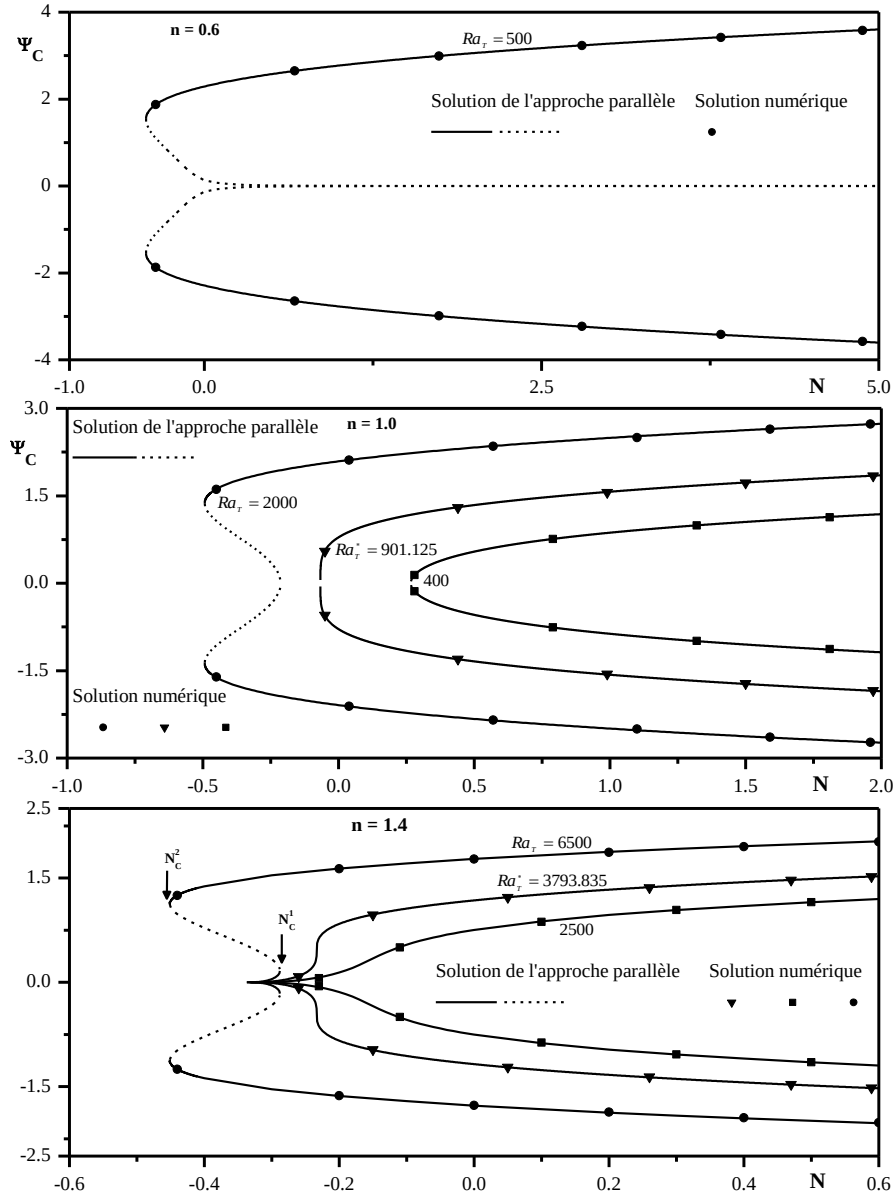

Figure 7. ψ_c as a function of N for Le = 2 and different values of Ra_T and n

5.2 Effect of N and n on fluid flow

The effect of the buoyancy ratio, N, on the value of stream function is illustrated on Figure 7 in terms of ψ_c variations vs. N for Le = 2 and different values of n and Ra_T. For the case of pure thermal convection (N = 0), the ensuing flow, driven only by the imposed temperature gradients, proceeds counter-clockwise. For n = 0.6, the results presented in Figure 7 are obtained for Ra_T = 500. According to this figure, convection is only attainable if the buoyancy ratio reaches a subcritical value $N_C^{Sub} = -0.4326$, above this critical value, the strength of the flow intensity is enhanced by an increase of N. For the

Newtonian fluid, the behavior of ψ_c depend strongly on the value of Ra_T. In fact, as shown in Figure 7, when $Ra_T \leq Ra_T^*$, the convection is supercritical and the corresponding supercritical buoyancy ratios are $N_C^{Sup} = -0.067$ for $Ra_T = Ra_T^* = 901.125$ and $N_C^{Sup} = 0.267$ for $Ra_T = 400$.

For $Ra_T > Ra_T^*$ the start of convection corresponds to a subcritical bifurcation arising when $N_C^{Sub} = -0.493$ for $Ra_T = 2000$. Here also, above these critical values, the strength of the flow intensity is enhanced by an increase of N. The corresponding results obtained for the case of a dilatant fluid (n = 1.4) is now considered. As observed from Figure 7, the convection is supercritical for any Ra_T and the presence of multiple solutions is noticed for $Ra_T > Ra_T^*$, where $Ra_T^* = 3793.835$. Thus, with the same values of the controlling parameters, three solutions of ψ_c are seen to be theoretically possible (indicated by solid and dashed lines) for $N_c^2 < N < N_c^1$ while the numerical results (depicted by blackened symbols) presented only two solutions for the same values of the controlling parameters.

5.3 Effect of Le and n on fluid flow

The influence of the Lewis number Le on the convection intensity ψ_c is shown in Figure 8 for N = -0.01, $Ra_T = 10^3$ and different values of n. Note that for low Lewis values (Le < 10^{-2}), the stream function is independent of this parameter. Then, by increasing Le, ψ_c decreases passing through a minimum at Le = 0.07, 0.95 and 32.0 for n = 0.6, 1 and 1.4 respectively, then increases and tends towards a constant value depending on n. For high Lewis values (Le > 10^2), the flow intensity again becomes independent of these values.

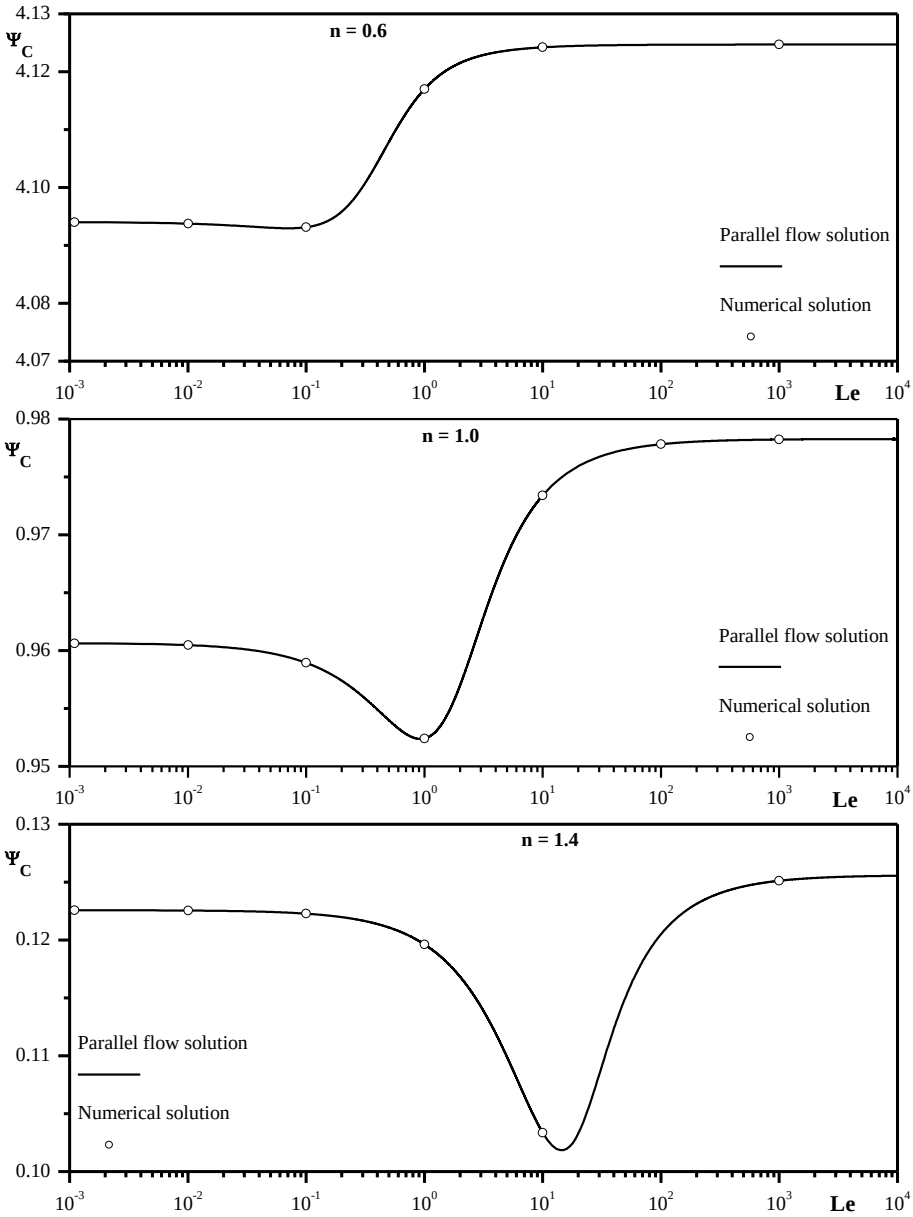

Figure 8. ψ_c as a function of Le for N = -0.01, $Ra_T = 10^3$ and different values of n

6. CONCLUSION

In this work, we presented a study on heat and mass transfers by Soret-driven natural convection of binary power-law fluid. The geometric configuration of the physical model is a tilted rectangular cavity subjected to vertical uniform fluxes of heat. The influence of the important controlling parameters including the thermal Rayleigh number, Ra_T, the

aspect ratio, A, the buoyancy ratio, N, The Lewis number, Le and the power law index, n, on the flow intensity and heat and mass transfer characteristics is analysed. The summary of the significant findings is:

1. The parallel flow approach verified in this investigation for the case of shallow layer (A >> 1) allowed us to develop an analytical solution for different governing equations of the problem.

2. The behavior of the fluid flow was found to be strongly dependent of the values of N and n. It has been proved that for:

- a dilatant fluid (n > 1): The convection phenomenon occurs for any value of Ra_T greater than zero provided that $N \geq N_1^*$. In the range of $N_2^* < N < N_1^*$, three solutions are observed to be possible for a given Ra_T. For $N \leq N_2^*$, convection becomes subcritical.
- a Newtonian fluid (n = 1): Convection is supercritical for $N \geq N^*$. When $N \leq N_2^*$, the convection becomes subcritical, for which the corresponding flow bifurcates from the rest state through convection state.
- a peudoplastic fluid (n < 1): Convection occurs via subcritical bifurcation regardless of the value of N.

REFERENCES

[1] Bahloul, A., Boutana, N., Vasseur, P. (2003). Double-diffusive and Soret-induced convection in a shallow horizontal porous layer. Journal of Fluid Mechanics, 491: 325-352. http://dx.doi.org/10.1017/S0022112003005524

[2] Bourich, M., Hasnaoui, M., Amahmid, A. (2004). Soret convection in a shallow porous cavity submitted to uniform fluxes of heat and mass. International Communications in Heat and Mass Transfer, 31(6): 773-782. http://dx.doi.org/10.1016/S0735-1933(04)00064-8

[3] Bourich, M., Hasnaoui, M., Amahmid, A., Er-Raki, M., Lagra, A., Mamou, M. (2016). Soret convection in a shallow porous cavity under a magnetic field and submitted to uniform fluxes of heat and mass. Journal of Applied Fluid Mechanics, 9(2): 741-749. http://dx.doi.org/10.18869/acadpub.jafm.68.225.21441

[4] Rebhi, R., Mamou, M., Hadidi, N. (2021). Onset of linear and nonlinear thermosolutal convection with Soret and DuFour effects in a porous collector under a uniform magnetic field. Fluids, 6(7): 243. https://doi.org/10.3390/fluids6070243

[5] Alloui, I., Benmoussa, H., Vasseur, P. (2010). Soret and thermosolutal effects on natural convection in a shallow cavity filled with a binary mixture. International Journal of Heat and Fluid Flow, 31(2): 191-200. http://dx.doi.org/10.1016/j.ijheatfluidflow.2009.11.008

[6] Lagra, A., Bourich, M., Hasnaoui, M., Amahmid, A., Er-Raki, M. (2018). Analytical and numerical study of Soret and Dufour effects on double diffusive convection in a shallow horizontal binary fluid layer submitted to uniform fluxes of heat and mass. Mathematical Problems in Engineering, 1-12. http://dx.doi.org/10.1155/2018/7946078

[7] Filahi, I., Bourich, M., Hasnaoui, M., Amahmid, A. (2020). Analytical and numerical study of Soret and Dufour effects on thermosolutal convection in a horizontal brinkman porous layer with a stress-free upper boundary. Mathematical Problems in Engineering, 1-17. http://dx.doi.org/10.1155/2020/4046570

[8] Mansour, A., Amahmid, A., Hasnaoui, M. (2008). Soret effect on thermosolutal convection developed in a horizontal shallow porous layer salted from below and subject to cross fluxes of heat. International Journal of Heat and Fluid Flow, 29(1): 306-314. http://dx.doi.org/10.1016/j.ijheatfluidflow.2007.07.002

[9] Wang, J., Yang, M., Zhang, Y. (2014). Onset of double-diffusive convection in horizontal cavity with Soret and Dufour effects. International Journal of Heat and Mass Transfer, 78: 1023-1031. http://dx.doi.org/10.1016/j.ijheatmasstransfer.2014.07.064

[10] Wang, J., Yang, M., Zhang, Y. (2015). Coupling–diffusive effects on thermosolutal buoyancy convection in a horizontal cavity. Numerical Heat Transfer, Part A: Applications, 68(6): 583-597. http://dx.doi.org/10.1080/10407782.2014.994412

[11] Charrier-Mojtabi, M.C., Elhajjar, B., Mojtabi, A. (2007). Analytical and numerical stability analysis of Soret-driven convection in a horizontal porous layer. Physics of Fluids, 19(12): 124104. http://dx.doi.org/10.1063/1.2821460

[12] Mojtabi, A. (2020). A new process for the determination of the Soret coefficient of a binary mixture under microgravity. International Journal of Thermal Sciences, 149: 106204. http://dx.doi.org/10.1016/j.ijthermalsci.2019.106204

[13] Mutschler, D., Mojtabi, A. (2020). Theoretical and numerical analysis of Soret-driven convection in a horizontal porous layer saturated by an n-component mixture: Application to ternary hydrocarbon mixture tetralin, isobutyl benzene, n-dodecane with mass fractions 0.8-0.1-0.1. International Journal of Heat and Mass Transfer, 162: 120339. http://dx.doi.org/10.1016/j.ijheatmasstransfer.2020.120339

[14] Benhadji, K., Vasseur, P. (2001). Double diffusive convection in a shallow porous cavity filled with a non-Newtonian fluid. International Communications in Heat and Mass Transfer, 28(6): 763-772. http://dx.doi.org/10.1016/S0735-1933(01)00280-9

[15] Khelifa, N.B., Alloui, Z., Beji, H., Vasseur, P. (2012). Natural convection in a horizontal porous cavity filled with a non-Newtonian binary fluid of power-law type. Journal of Non-Newtonian Fluid Mechanics, 169: 15-25. http://dx.doi.org/10.1016/j.jnnfm.2011.11.002

[16] Rebhi, R., Mamou, M., Hadidi, N. (2021). Bistability bifurcation phenomenon induced by non-Newtonian fluids rheology and thermosolutal convection in Rayleigh–Bénard convection. Physics of Fluids, 33(7): 073104. https://doi.org/10.1063/5.0051058

[17] Saeed, A., Karimi, N., Hunt, G., Torabi, M., Mehdizadeh, A. (2020). Double-diffusive transport and thermodynamic analysis of a magnetic microreactor with non-Newtonian biofuel flow. Journal of Thermal Analysis and Calorimetry, 140(3): 917-941. http://dx.doi.org/10.1007/s10973019-08629-3

[18] Amari, B., Vasseur, P., Bilgen, E. (1994). Natural convection of non-Newtonian fluids in a horizontal porous layer. Wärme-und Stoffübertragung, 29(3): 185-193. http://dx.doi.org/10.1007/BF01548603

[19] Bihiche, K., Lamsaadi, M., Hasnaoui, M. (2020).

Multiple steady state solutions for double-diffusive convection in a shallow horizontal rectangular cavity uniformly heated and salted from the side and filled with non-Newtonian power-law fluids. Journal of Non-Newtonian Fluid Mechanics, 283: 104349. http://dx.doi.org/10.1016/j.jnnfm.2020.104349

[20] Li, Y., Yang, M., Zhang, Y. (2021). Bifurcation analysis of coupling thermosolutal convection induced by a thermal and solutal source in a horizontal cavity. International Communications in Heat and Mass Transfer, 126: 105455. http://dx.doi.org/10.1016/j.icheatmasstransfer.2021.105455

[21] Makayssi, T., Lamsaadi, M., Naimi, M., Hasnaoui, M., Raji, A., Bahlaoui, A. (2008). Natural double-diffusive convection in a shallow horizontal rectangular cavity uniformly heated and salted from the side and filled with non-Newtonian power-law fluids: the cooperating case. Energy conversion and Management, 49(8): 2016-2025. http://dx.doi.org/10.1016/j.enconman.2008.02.008

[22] Kefayati, G.R., Tang, H. (2019). Three-dimensional Lattice Boltzmann simulation on thermosolutal convection and entropy generation of Carreau-Yasuda fluids. International Journal of Heat and Mass Transfer, 131: 346-364. http://dx.doi.org/10.1016/j.ijheatmasstransfer.2018.11.076

[23] Siginer, D.A., Valenzuela-Rendon, A. (2000). On the laminar free convection and instability of grade fluids in enclosures. International Journal of Heat and Mass Transfer, 43(18): 3391-3405. https://doi.org/10.1016/S0017-9310(99)00357-9

[24] Turki, S. (1990). Contribution to numerical study of natural and mixed convection heat transfers in confined non-Newtonian fluids. Doctoral dissertation, Ph. D. thesis, CNAM, Paris, France.

[25] Patankar, S.V. (1980). Numerical Heat Transfer and Fluid Flow. Hemisphere, Washington, DC, USA. http://dx.doi.org/10.1201/9781482234213

[26] Lamsaadi, M., Naimi, M., Hasnaoui, M. (2006). Natural convection heat transfer in shallow horizontal rectangular enclosures uniformly heated from the side and filled with non-Newtonian power law fluids. Energy conversion and Management, 47(15-16): 2535-2551. http://dx.doi.org/10.1016/j.enconman.2005.10.028

[27] Ouriemi, M., Vasseur, P., Bahloul, A., Robillard, L. (2006). Natural convection in a horizontal layer of a binary mixture. International Journal of Thermal Sciences, 45(8): 752-759. http://dx.doi.org/10.1016/j.ijthermalsci.2005.11.004

[28] Sibony, M., Mardon, J.C.I. (1982). Numerical Analysis II, Approximation and Differential Equations, Hermann, Paris.

[29] Gourdin, A., Boumahrat, M. (1989). Applied numerical methods. Technique and Documentation-Lavoisier, Paris.

[30] Bejan, A. (1983). The boundary layer regime in a porous layer with uniform heat flux from the side. International Journal of Heat and Mass Transfer, 26(9): 1339-1346. http://dx.doi.org/10.1016/S0017-9310(83)80065-9

[31] Turan, O., Lai, J., Poole, R.J., Chakraborty, N. (2013). Laminar natural convection of power-law fluids in a square enclosure submitted from below to a uniform heat flux density. Journal of Non-Newtonian Fluid Mechanics, 199: 80-95. https://doi.10.1016/j.jnnfm.2013.06.002

[32] Ozoe, H., Churchill, S.W. (1972). Hydrodynamic stability and natural convection in Ostwald-de Waele and Ellis fluids: The development of a numerical solution. AIChE Journal, 18(6): 1196-1207. http://dx.doi.org/10.1002/aic.690180617

NOMENCLATURE

A	aspect ratio of the enclosure
C_T	dimensionless temperature gradient in the *x*-direction
C_S	dimensionless concentration gradient in the *x*-direction
D	isothermal diffusion coefficient, m^2/s
g	gravitational acceleration, m/s^2
H'	height of the layer, m
k	consistency index of the fluid, $Pa.s^n$
Le	Lewis number
L'	length of the rectangular enclosure (m)
N	buoyancy ratio
n	power-law index
$\overline{Nu}$	average Nusselt number
Pr	Prandtl number
q'	constant heat flux per unit area, W/m^2
Ra_T	thermal Rayleigh number
S	dimensionless concentration
S'_c	reference concentration at the geometric center of the enclosure, kg/m^3
ΔS^*	characteristic concentration, kg/m^3
$\overline{Sh}$	average Sherwood number
T	dimensionless temperature
T'_c	reference temperature at the geometric center of the enclosure, K
ΔT^*	characteristic temperature, K

Greek symbols

α	fluid thermal diffusivity, $m^2.\ s^{-1}$
λ	fluid thermal conductivity, $W.m^{-1}.K^{-1}$
μ_a	dimensionless apparent viscosity of fluid
ρ	density of fluid, kg/m^3
ψ	dimensionless stream function

Subscripts

c	value relative to the centre of the cavity